Acidic properties of Al-rich ZSM-5 crystallized in strongly acidic fluoride medium

Diandian Shi, Guangying Fu, Ahmed Omran, Kok-Giap Haw, Liangkui Zhu, Ruiqin Ding, Qiaolin Lang, Songxia Wang, Qianrong Fang, Shilun Qiu, et al.

Acidic properties of Al-rich ZSM-5 crystallized in strongly acidic fluoride medium[#]

Diandian Shi,[a,b] Guangying Fu,[a] Ahmed Omran,[c] Kok-Giap Haw,[b] Liangkui Zhu,[b] Ruiqin Ding,[a] Qiaolin Lang,[a] Songxia Wang,[a] Qianrong Fang,[b] Shilun Qiu,[b] Xiaobo Yang,[a,**] and Valentin Valtchev [a,c,*]

[a] Qingdao Institute of Bioenergy and Bioprocess Technology, Chinese Academy of Sciences, Laoshan District, Qingdao CN-266101, China

[b] State Key Laboratory of Inorganic Synthesis and Preparative Chemistry, Jilin University, Changchun CN-130012, China

[c] Normandie University, ENSICAEN, UNICAEN, CNRS, Laboratoire Catalyse et Spectrochimie, 6 Marechal Juin, F-14050 Caen, France

[*] Corresponding author.

[**] Corresponding author.

E-mail addresses: valentin.valtchev@ensicaen.fr, yangxb@qibebt.ac.cn.

[#] Dedicated to Prof. Avelino Corma on the occasion of his 70th birthday.

Abstract

The fluoride medium synthesis of zeolites, especially in the strongly acidic regions, yields products with unique characteristics such as ultra-hydrophobic surfaces and defect-free lattices. However, it is often difficult to incorporate aluminum into the framework of zeolites in this medium, limiting the acquisition and development of catalytic materials. The present paper shows that inter-zeolite transformation is efficient for obtaining ZSM-5 zeolites with lower Si/Al ratios in a strongly acidic fluoride medium. The critical point is that the parent zeolites can retain some locally ordered fragments during their dissolution, including framework Al atoms, and incorporate them into the ZSM-5 product. The acidic properties of the trans-crystallization products obtained in an acidic medium display significant differences from the traditional ZSM-5 with a similar Si/Al ratio in the amounts, strength, and types of the acid sites; thus, they behave differently in typical acid-catalyzed reactions, such as dehydration of alcohols.

Keywords: zeolite crystallization in acidic medium; inter-zeolite thansfromation in acidic medium; Al-rich zeolite in fluoride medium; unique acidity of Al-rich ZSM-5 through IZT; catalysis of Al-rich ZSM-5 through IZT

1. Introduction

Zeolites are the most important sorbents and catalysts in the oil refinery and petrochemical industry, owing to their uniform microporous structures delineated by the crystalline framework lattices. And nowadays they increasingly find new applications in renewable energy, environmental protection, and advanced functional materials.[1, 2] However, working out of the traditional “comfort” zone, the new applications require zeolites possessing novel structural

and surface-chemical properties and exceptional (hydro-)thermal stability. In turn, the synthetic chemistry of zeolites needs to be reviewed and improved.[3, 4]

Aluminium atoms in the framework of zeolites introduce negative charges, which are counter-balanced by extra-framework cations, such as protons, and generate Brønsted acidity, while defects associated with framework Al atoms are Lewis acid sites.[5] Thus, zeolites have been used as solid acid catalysts since 1960s due to their high catalytic activities, environmentally benign nature, and excellent thermal stability. The catalytic activity is determined mainly by the strength and number of their acid sites. The density of acid sites in the framework is directly related to the aluminium content; thus, the catalytic properties may be tailored by altering the aluminium content of zeolites.[6] Acid catalysed reactions, such as cracking, isomerization, alkylations,[7] hydrocracking,[8] as well as methanol conversions to olefin (MTO)[9] or gasoline (MTG), and alcohol dehydration[10, 11] or carbonylation are the key processes in oil refining,[12] petrochemistry,[13] and fine chemical production.[14]

A significant breakthrough, as initiated by the researchers at Muhlouse and Valencia, in the field of zeolite synthesis occurred when hydroxyl anion as a mineralizer was replaced by fluoride, extending the synthesis from the traditional basic conditions (pH = 9~14) to the neutral medium (pH = 5~8).[15-17] The fluoride ion presents several advantages as a mineralizer, such as the generation of high-silica zeolites, large crystal sizes, hydrophobic surfaces, and substantially defect-free lattices.[18, 19] These advantages become even more pronounced when the pH of the synthetic medium expands further to the strongly acidic region.[20] We have recently demonstrated the synthesis and morphology control methods for silicalite-1, high-silica ZSM-5, and some other microporous silicate materials in the pH range of 2~5.[20-23]

However, it is difficult to incorporate active catalytic metals whose oxo-anions have higher isoelectronic points (IEP) in the neutral and acidic fluoride medium framework. Unfortunately, Al as one of the most common framework elements in zeolites, is hardly to be incorporated under acidic conditions since the aluminate ion has pH_{IEP} = 7.7. [24] In addition, the ease of substitution decreases with increasing stability of the corresponding fluoro-complexes in the solution. The great stability of fluoro-aluminate complexes reduces the activity of the "useful species" and hinders the rapid incorporation of Al atoms.[25] Therefore, it becomes challenging to incorporate a sufficient amount of framework Al into zeolites in an acidic fluoride medium.[20] Thus, the highly ordered and defect-free lattice structure obtainable in an acidic medium is hardly combined with a large concentration of acid sites useful in many catalytic applications.[26]

Inter-zeolite transformations (IZT), employing industrial zeolites as silica-alumina sources to generate another target zeolite, has recently drawn much attention.[27-31] The zeolite crystallization by IZT is faster and yields high.[32-34] The method can also provide pathways to synthesize zeolites with specific frameworks and compositions that are not possible with conventional silica and alumina sources. Rimer et al. have pointed out that local ordering of the precursor could facilitate heterogeneous nucleation during IZT. The nature of dissolved species is unknown but could be monomers, oligomers, or composite building units (CBUs) and rings that retain some "memory" of the parent.[35, 36] Furthermore, Dusselier et al. studied several IZT systems, and revealed that aluminum from the parent is the key to drive the inherently fast nucleation; and is assembled into the product frameworks with various manners at latter stages of the crystal growth.[37] Inspired by this theory, we hypothesized that IZT of Al-containing zeolites in an acidic medium may transfer -Al-O-Si- linkages from parents to products,

especially when they possess common CBUs. Setting a relatively low Si/Al ZSM-5 zeolite as a target, we envisage that it would be advantageous to use the other members of the pentasil family, such as the ones with ***BEA**, **FER**, **MOR**-type frameworks as the parents. Here we refer to a broader definition of pentasils rather than to restrict the concept solely within the stacking polymorphous of the pentasil layer as a periodic building unit (PerBU) between the end members **MFI** and **MEL**.[38] **MFI**, **FER**, and **MOR** have in common that they are all built up from the (*5-1*) secondary building unit (SBU). ***BEA** is a disordered structure that does not have an SBU, but it is built from a combination of (*5-1*) and (*6-2*) units. Furthermore, **MFI**, ***BEA**, **FER,** and **MOR** have as CBU a common *mor* structural motif (Scheme 1). Therefore, we employed these pentasil-type zeolites as the initial silica-alumina sources for our acidic-medium synthesis. For the sake of comparison, we have also used a zeolite, USY-**FAU**, which does not possess the (*5-1*) unit. The objective is to trace the way to synthesize heteroatom-containing zeolites under an acidic fluoride medium.

Furthermore, we compare the acid site concentrations, types, and strengths of ZSM-5 obtained through IZT in the acidic medium with a conventional, basic-medium synthesized ZSM-5. The results show that IZT materials possess unique acidic properties in terms of the framework integrity, the amounts, and the strength distributions of Brønsted and Lewis acid sites, which lead to different performances in a typical acid-catalysed reaction, i.e., the dehydration of short-chain alcohols.

2. Experimental

2.1 Materials and reagents

All chemicals and reagents were used as purchased without further purification. They were tetrapropylammonium bromide (TPABr 98%, Sigma-Aldrich), hydrofluoric acid (HF 40% a.q., J&K Scientific Co., Ltd.), ammonium fluoride (NH_4F 98%, Sigma-Aldrich), Ludox AS-40 (40wt% SiO_2, Sigma-Aldrich), TPAOH (25% a.q., Kente Catalysts Inc.), NaOH (AR, Sinopharm Chemical Reagent Co., Ltd), $NaAlO_2$ (CP, Sinopharm Chemical Reagent Co., Ltd). Deionized water was used in all experiments.

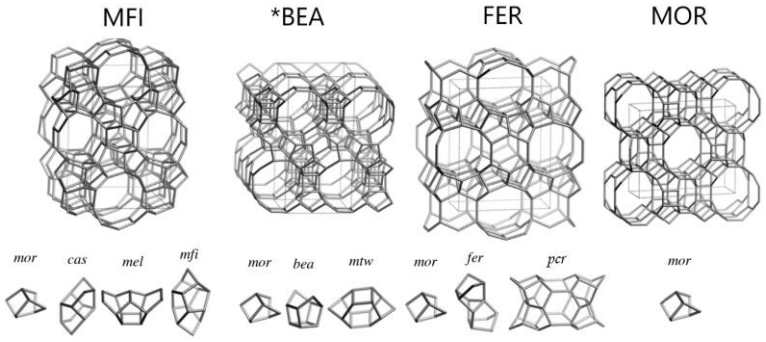

Scheme 1. The frameworks **MFI**, ***BEA**, **FER**, **MOR** and their respective composite building units (CBUs), where *mor* is a common CBU of these zeolites.

Four zeolite materials were chosen as the parents for IZT experiments: NH_4-ferrierite, Zeolyst; zeolite H-beta, Sanbang Chemicals; H-mordenite, Nankai University Catalyst Co.; high-silica zeolite H-Y (USY, CBV 760), Zeolyst. The basic characterizations of these materials, including

XRD, SEM, and N_2-adsorption isotherms, are detailed in the Supplementary Information in Figures S1-S3 and Table S1.

2.2 Synthesis

Synthesis of ZSM-5 via Inter-zeolite transformation: 1.5 g of the parent zeolite material, which had been calcined at 550ºC for 6 h, was added into a solution of 1.019 g TPABr in 18 g deionized water. The mixture was stirred at room temperature for 3 hours to homogenize. Then 0.457 g (40%) HF and 0.162 g NH_4F were diluted with a small amount of water and added dropwise. Finally, the obtained slurry, which had a pH value of around 3.0, was transferred into a 50 mL Teflon-lined stainless-steel autoclave and subjected to hydrothermal treatment at 160ºC for 6 days. For the IZT of zeolite H-Y (USY), an additional series of experiments kinetics was performed, by varying the crystallization time between 1 and 18 days. After the hydrothermal treatments, the solid products were collected with vacuum filtration, washed thoroughly with deionized water until a near-neutral pH, and dried overnight at 60ºC. Calcination of the samples was performed at 550ºC for 6 h in air. The ZSM-5 samples were denoted as B-Z, F-Z, M-Z, and Y-Z, with zeolite beta, ferrierite, mordenite, and zeolite Y as the parents. The molar compositions of these syntheses were: 21 SiO_2: Al_2O_3: 995 H_2O: 4.3 TPABr: 4.3 NH_4F: 8.9 HF (B-Z), 18 SiO_2: Al_2O_3: 870 H_2O: 3.6 TPABr: 3.8 NH_4F: 7.8 HF (F-Z), 17 SiO_2: Al_2O_3: 790 H_2O: 3.6 TPABr: 3.4 NH_4F: 7.1 HF (M-Z), 51 SiO_2: Al_2O_3: 2400 H_2O: 10 TPABr: 10.4 NH_4F: 21.7 HF (Y-Z), i.e., in general at ca. TO_2: 0.2 TPABr: 0.2 NH_4F: 0.4 HF: 40 H_2O.

Synthesis of a reference ZSM-5 sample in basic medium: The initial gel had the molar composition $3.25Na_2O$: $0.6Al_2O_3$: $30SiO_2$: $958H_2O$: 9TPAOH. At first, 0.1413 g NaOH, 0.0656 g $NaAlO_2$, and 4.8808 g 25% TPAOH were dissolved in 6.0317 g water. 3.004 g Ludox AS-40 was added dropwise. The mixture was stirred further at room temperature for 6 h. Nanosized silicalite-1[39] seeds (2% weight portion of SiO_2) were added, and stirred for another 30 min. The obtained mixture was transferred into a 50 mL autoclave, sealed, and heated at 180ºC for 2 days.

2.3 Characterization

Powder X-ray diffraction (XRD) data of all materials were collected using a PANalytical B.V. Empyrean powder diffractometer with Cu Kα radiation (λ = 1.5418 Å, 40 kV, 40 mA) over the range of $2\theta = 4.0 - 40.0°$ with a scanning speed of $0.026° \ s^{-1}$.

Thermogravimetric analysis (TGA) was carried out with a SHIMADZU DTG-60 thermal analyzer system in 30 $mL \cdot min^{-1}$ air flow with a heating rate of 10°C/min from 30 to 600°C.

Scanning electron microscopy (SEM) data were acquired using a JEOL JSM7400F microscope and a MIRA-LMH (TESCAN) scanning electron microscope (SEM). Both of them are equipped with field emission guns. The Si/Al ratios of samples were determined by energy-dispersive X-ray (EDS) analysis.

Nitrogen adsorption measurements were performed using a Micromeritics ASAP 2040 automated gas adsorption analyzer at 77 K. Calcined samples were outgassed at 300°C for 12 h prior to analysis. The microporous volume (V_{mic}, cm^3g^{-1}) was obtained from the t-plot analysis based on the Harkins-Jura equation.

Elemental analysis of Si and Al was performed using an Optima 3300 DV ICP-AES of Perkin-Elmer. The powder sample was at first digested in a aqueous solutions of HF and HNO_3/HCl, cooked with additional H_3BO_3 to remove the excessed HF, and diluted with water before the analysis.

^{27}Al and ^{29}Si MAS NMR experiments were performed on Bruker AVANCE III 600 spectrometer equipped with a 4 mm triple resonance probe operating at a resonance frequency of 156.4 MHz and 119.2 MHz, respectively. ^{27}Al MAS NMR spectra were recorded using a small-flip angle technique with a pulse length of 0.5 μs (< π/12), a 1s recycle delay and a spinning rate of 14 kHz. ^{29}Si MAS NMR spectra with high-power proton decoupling were recorded at a spinning rate of 10 kHz, a π/4 pulse length of 2.6 μs, and a recycle delay of 60 s. The chemical shifts of ^{27}Al and ^{29}Si MAS were referenced to 1 mol/L aqueous $Al(NO_3)_3$ and TMS, respectively. ^{19}F MAS NMR was carried out at a resonance frequency of 564.5 MHz using a 4 mm HX double-resonance MAS probe at a spinning rate of 15 kHz. ^{19}F MAS NMR spectra were recorded with a π/2 pulse length of 3.5 μs and a 10 s recycle delay. The chemical shifts were referenced to $CFCl_3$.

FTIR spectra of the zeolites' framework vibrations were recorded on KBr pellets using Brucker Vertex 70V Spectrometer at a spectral resolution of 4 cm^{-1}. The equipment, including the sample chamber, was evacuated to below 1 hPa. The *in situ* FTIR studies were performed on self-sustaining pellets of a density of 20 mg/cm^2, which are enclosed in a gas-tight and heated cell with CaF_2 windows. Spectra of the -OH vibrations were recorded under vacuum at RT after dehydration at 450^{o}C for 30 min. Spectra of samples with adsorbed pyridine were recorded after exposure to pyridine vapor at RT, and evacuation at 100^{o}C for 1 hour.

NH_3-TPD was carried out in a flowing system operating at atmospheric pressure. 100 mg sample (60-100 mesh) were loaded in a quartz tube of ϕ = 4 mm, and dehydrated in 50 mL/min He at 350^{o}C for 1 h; then NH_3 was saturated at 100^{o}C and flushed with He for 0.5 h. The temperature-programmed desorption was then performed at 10^{o}C/min to 800^{o}C. The amount of desorbed NH_3 was recorded using a TCD.

Catalytic tests were carried out in a plug-flow fixed-bed microreactor with a tubular quartz reactor of ϕ = 5 mm operating at the atmospheric pressure. 200 mg catalysts (60-100 mesh) were loaded and dehydrated in 50 mL/min Ar low at 350^{o}C for 0.5 h. The reaction tests for dehydration of methanol, ethanol, and 1-propanol were performed at various temperatures with feeds of 0.016 mL/min MeOH, 0.005 mL/min EtOH and 0.005 mL/min in 50 mL/min Ar (STP), respectively. The steady-state conversions and selectivity were taken from data collected using an online GC with an FID in 0.5 to 2.5 h time-on-stream.

3. Results and discussion

3.1 ZSM-5 crystal growth kinetics

Four commercially available zeolites, i.e., zeolite H-beta, H-ferrierite, H-mordenite, and zeolite H-Y (USY), were chosen as the parent materials for inter-zeolite transformation in a strongly acidic fluoride medium. Their basic characteristics are shown in the Supplementary Information (XRD, SEM, and N_2 sorption isotherms in Figure S1-S3 and Table S1, respectively). They all show good phase purity. The crystals of H-Y have a well-developed octahedral shape and have

sizes around 1 μm; the other samples contain irregular agglomerates built up of smaller crystallites. The Si/Al ratios of the pentasil materials are about 10. The USY has a Si/Al ratio of 28.

In the presence of TPABr and HF/NH_4F in the slurries of pH ~3, all four parent zeolites transform to ZSM-5 under hydrothermal treatments at 160°C, but the transformation of H-Y shows obviously different kinetics from the other three pentasil-type zeolites. Figure 1a shows the XRD patterns of the recovered solid products after 6 days of hydrothermal treatments. It shows that the inter-zeolite transformations of the pentasil zeolites, i.e., from zeolite ferrierite, beta, and mordenite to ZSM-5, have completed in 6 days; while the 6-day product from H-Y just shows traces of **MFI**-type material. Upon prolonged time of hydrothermal treatment, H-Y can transform to ZSM-5, too. Figure 1b shows the XRD patterns of the solids recovered from 1 to 18 days. SEM pictures of these products are shown in Figure 2. H-Y dissolves in the first 3 days; it starts to crystallize on the 6th day; and the crystallization completes until the 18th day. SEM pictures in Figure 3 show the morphologies of the solid products at the 6th and 13 th days, revealing big crystals growing in the small particles of gels. (N_2 adsorption/desorption isotherms in figure S5, and TGA in Figure S6 of the samples taken along the 18-day hydrothermal treatments in the Supplementary Information). It should be noted that the Si/Al ratio of the parent H-Y is even higher than that of pentasil samples. Hence, we exclude that it may play a role in the delayed synthesis. This result is strong proof that the framework topology of parent zeolite indeed influences the crystallization process.

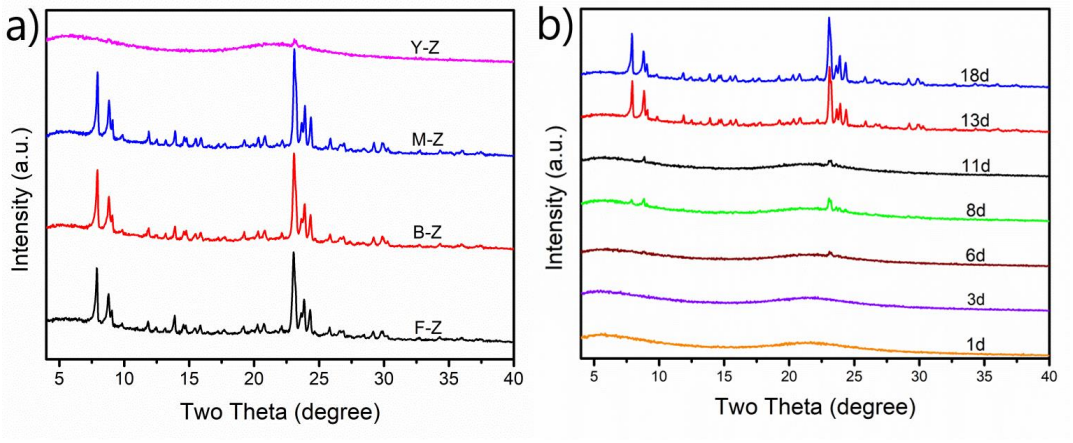

Figure 1. Powder XRD patterns of the inter-zeolites transformation products obtained in the acidic medium after hydrothermal treatments at 160°C: a) in 6 days using zeolite Y, mordenite, beta and ferrierite as the parents; and b) in 1 to 18 days using zeolite Y as the parent.

Control experiments without using a parent zeolite, starting instead from a freshly prepared amorphous hydrogels with Si/Al =10, 15 and 30, at pH = 3, do not produce pure ZSM-5 in 6 days nor in 13-14 days. Instead, at Si/Al = 10, crystalline aluminium hydroxide fluoride was ($Al(OH)_{1.5}F_{1.5}(H_2O)_{0.375}$) obtained together with amorphous gels. At Si/Al = 15, AlF_3 crystals appear together with badly crystallized **MFI** zeolite. At Si/Al =30, **MFI** zeolite becomes the main product in 14 days, but the aluminium hydroxide fluorid still appear (Figure S7). Pure and Al-rich ZSM-5 cannot be synthesized directly from amorphous gels at the presence of HF.

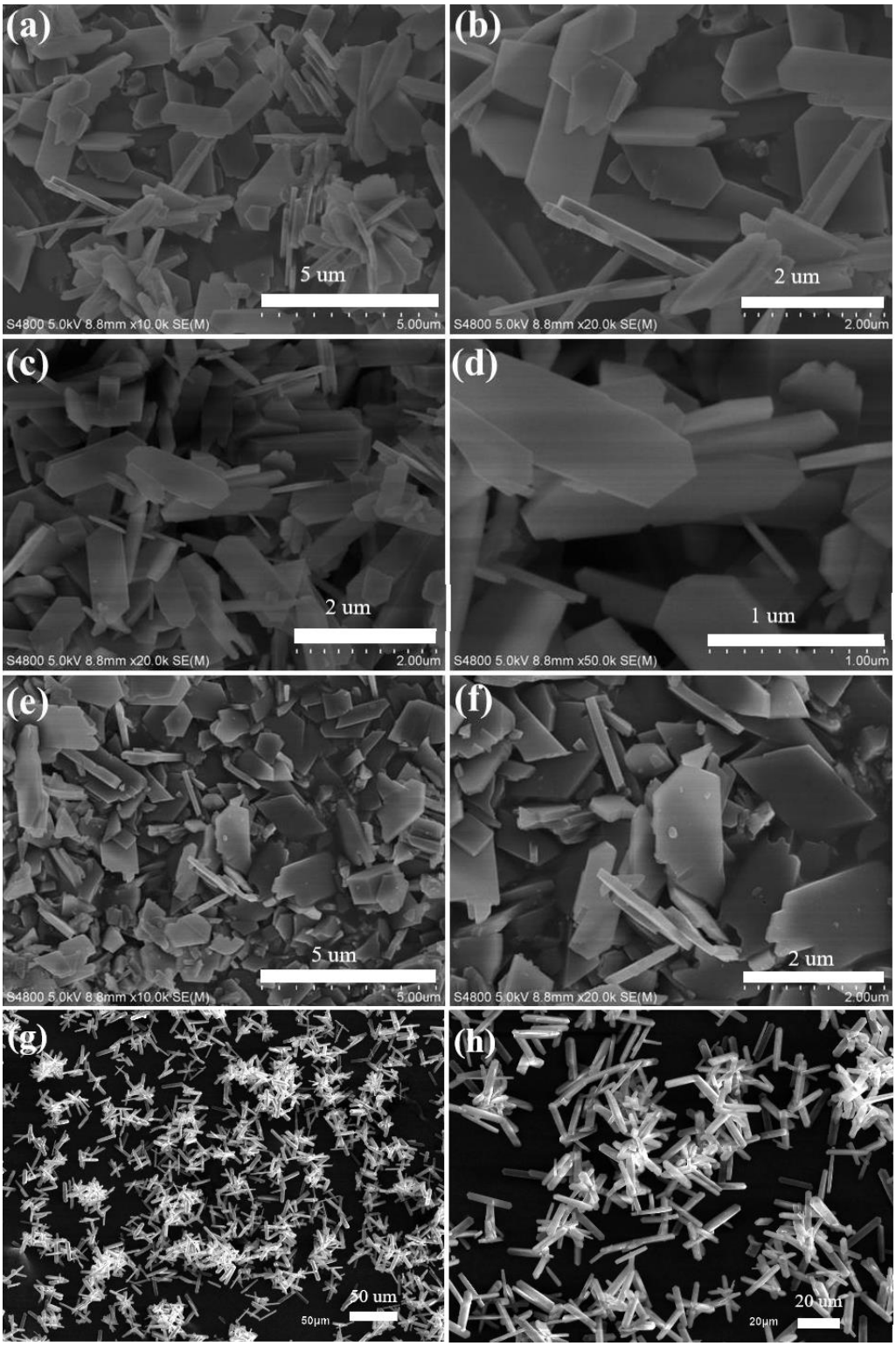

Figure 2. SEM images of the inter-zeolite transformation products in the acidic medium: (a,b) F-Z, ZSM-5 out of ferrierite; (c,d) B-Z, ZSM-5 out of zeolite beta; (e,f) M-Z, ZSM-5 out of mordenite; (g,h) Y-Z, ZSM-5 out of USY.

Figure 4 shows the N_2 adsorption/desorption isotherms of the inter-zeolite transformation products. They are Type I isotherms, showing similar micropore volumes of 0.15-0.16 cm^3g^{-1}, and BET specific surface areas close to 400 m^2g^{-1}. These characteristics correspond to a highly

crystalline **MFI**-type zeolite. In terms of N_2 adsorption amount and micropore volume, the 18-day ZSM-5 product Y-Z is similar to the 6-day products out of the pentasil materials, B-Z, M-Z, and F-Z, despite the different Si/Al ratios (Table 1).

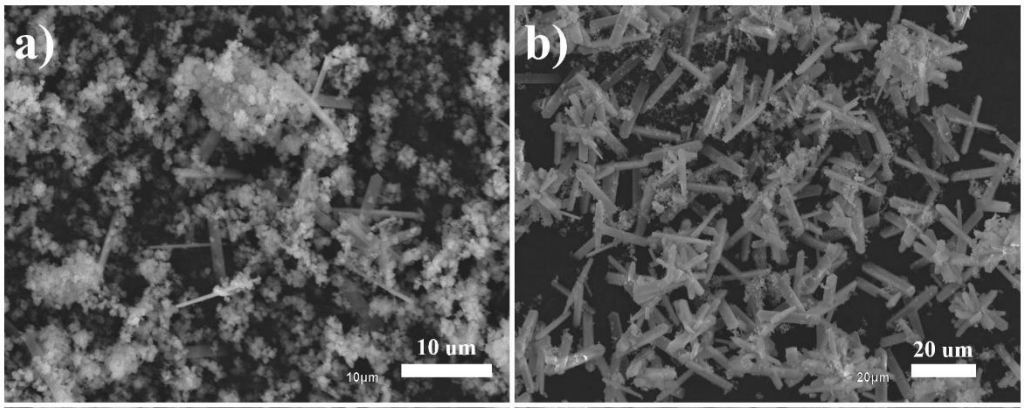

Figure 3. SEM images of the solid products in 6 and 13 days of the Y-Z experiment.

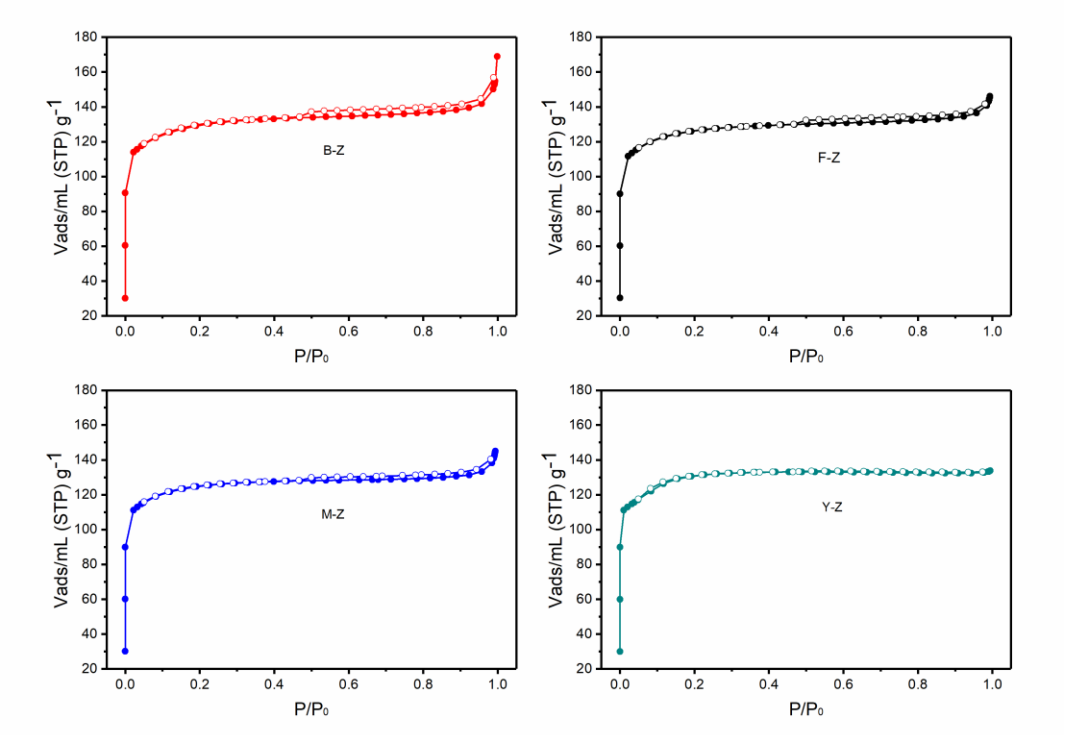

Figure 4. N_2 adsorption/desorption isotherms of ZSM-5 obtained by the inter-zeolite transformation in the acidic medium: B-Z, out of zeolite beta; F-Z out of ferrierite; M-Z out of mordenite; Y-Z out of USY.

The SEM pictures of the IZT products are shown in Figure 2. ZSM-5 crystals obtained from the parent ferrierite (F-Z), zeolite beta (B-Z), and mordenite (M-Z) in 6 days are thin plates with short edges along the b-axis. The straight channel of **MFI**-type material is running along the b-axis. Thus, the obtained morphology is favourable for catalytic applications. We attribute the plate-like morphology to the presence of the fluorine ion in the system as was shown in a previous study.[40] F-Z and B-Z plates exhibit a length around 2 µm. The length of M-Z crystals reaches ca. 5 µm, but many plates are broken. The 18-day Y-Z crystals show a different

morphology. They are much bigger with a size of ca. 20 μm in length, with high a/b aspect ratios. The different crystals size is a function of the number of nuclei in the system. Smaller crystals are obtained in systems with more abundant nucleation since crystallization stops with the exhausting of the nutrient pool. Our data show that the nucleation in the systems containing pentasil-type zeolites is more abundant and thus the ultimate crystals size smaller.

In contrast, the number of viable nuclei is limited, and the ultimate crystal size is larger in the H-Y system. The crystal growth rate in the H-Y system is slower, which we attribute to the dissolved species which do not contain elements of pentasil structure. Consequently, the 18-day Y-Z are bigger crystals with a size that is commonly seen in the fluoride medium synthesis of zeolites. Here the bigger crystals indicate a more complete dissolution of the starting source, bypassing the initial benefit of elements being well mixed by IZT.

Table 1. Si/Al ratios and texture properties of the inter-zeolite transformation products in the acidic medium.

Sample	Si/Al SEM-EDS	Si/Al ICP-AES	S_{BET} [m^2g^{-1}]	V_{micro} [cm^3g^{-1}]	Yield/%[a]
B-Z	16	22.7	391	0.15	78.7
F-Z	18	20.2	379	0.16	87.3
M-Z	17	21.8	374	0.16	78.0
Y-Z	34	40.0	393	0.15	76.3

[a] Yield% = $m_{calcined\ ZSM\text{-}5}/m_{calcined\ parent\ zeolite} * 100$

Regarding the inherently fast transformations of the parent pentasils to ZSM-5, and the retarded formation of ZSM-5 out of H-Y under the same conditions, it is critical that the parent zeolites retain some locally ordered fragments, including framework Al atoms, and incorporate them into the ZSM-5 product after their dissolution.

3.2 Al siting and acidity of the inter-zeolite transformation products

^{29}Si and ^{27}Al MAS NMR spectra of the inter-zeolite transformation products, and the reference ZSM-5 sample synthesized according to a traditional basic recipe (XRD in Figure S8 in the Supplementary Information), are shown in Figure 5.

Unexpectedly, the ^{29}Si MAS NMR spectra of the IZT-products show not-much better resolutions than the reference sample, only two broad Q^4 ($Si\text{-}(OSi)_4$) bands at ca. -114 and -112 ppm, and a broad Q^3 ($AlO\text{-}Si\text{-}(OSi)_3$) band ca. -106 ppm are recognizable. The reference has similar Q^4 signals and a broader band extending in the Q^3 and Q^2 region.[41, 42] The high spectral resolution for **MFI**-zeolites synthesized in the acidic medium that is associated with highly-ordered and defect-free crystal lattices,[20, 21] is not attained for the IZT products. Only slightly better than the basic reference, the structures of the IZT products still contain disorders. The values of the framework Si/Al ratios cannot be reliably extracted from these spectra due to the limited resolutions.

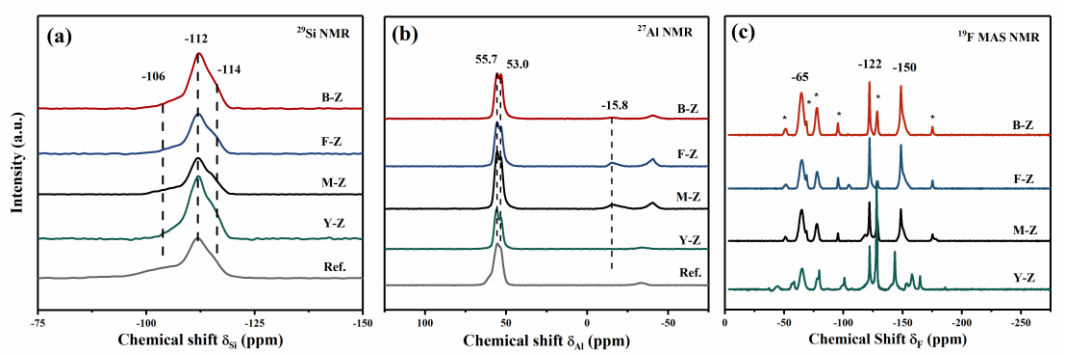

Figure 5. ^{29}Si, ^{27}Al and ^{19}F MAS NMR of the inter-zeolite transformation products, in comparison with the reference ZSM-5 synthesized in a traditional basic medium.

^{27}Al MAS NMR shows that the IZT products contain tetrahedrally bonded Al, similar to and better ordered than the reference, with chemical shifts at 56 and 53 ppm. Noteworthy, the products out of the pentasil-type parents have additional polymeric AlO_6-octahedra showing a broad NMR peak at ca. -15 ppm. The portions of the peak are 2.6% in B-Z, 7.6% in F-Z and 10.4% in M-Z. The presence of extra-framework aluminium is due to the fact that the Si/Al ratio on the zeolite sources used for IZT was about 10. The minimum Si/Al ratio for an **MFI**-type zeolite synthesised with TPA^+ is 23, which corresponds to 4 TPA^+ cations in a unit cell of 96 T-atoms. The IZT product out of H-Y does neither show this peak, which confirms that the excess alumina content in the initial zeolite is the reason for extra-framework aluminium species in B-Z, F-Z, and M-Z.

In ^{19}F MAS NMR spectra of the IZT products in Figure 5, three types of 3 types of fluorine atoms are recognizable among the spinning sidebands for the pentasils to ZSM-5 products: the one that occupies the well-known [$4^1 5^2 6^2$] cage at -65 ppm,[43] the one that are multiply and strongly bonded in Si-F_x at -122 ppm[23, 44] and in Al-F_x at -150 ppm.[45, 46] The latter two types of F atoms confirm the existences of not-fully 4-connected T atoms, and are in accordance with the FTIR and acidity characterizations in below paragraphs. The Y-Z product shows again a more complecated spectrum, showing the existences of more Si-F_x and Al-F_x species, i.e., a more distorted framework.

Y-Z possesses a better connectivity of framework AlO_4-tetrahedra than B-Z, F-Z and M-Z, but it has another kind of structural imperfection, as FTIR reveals in Figure 6a. Compared with the spectra in the framework vibrational region of the IZT products issued from the pentasils, for Y-Z the vibrations of the symmetric bending δ(O–Si–O) at 475 cm^{-1}, δ (Si–O–Si) at 725 cm^{-1}, the asymmetric stretching ν (Si–O–Si) at 1100 cm^{-1}, as well as the ring-breath vibrations which is typical for ZSM-5 at around 550 cm^{-1} are all obviously broader.[47-49] The framework of Y-Z is distorted.

The Si/Al ratios of the IZT-products have been analysed by ICP-AES and EDS methods, and are listed in Table 1. According ICP, the ZSM-5 products out of the pentasils have Si/Al ratios of ca. 20, Y-Z has ca. 40. All these values are higher than the respective parents. The corresponding values of EDS analyses are significantly lower than ICP, due to enrichments of Al atoms towards crystal shells.

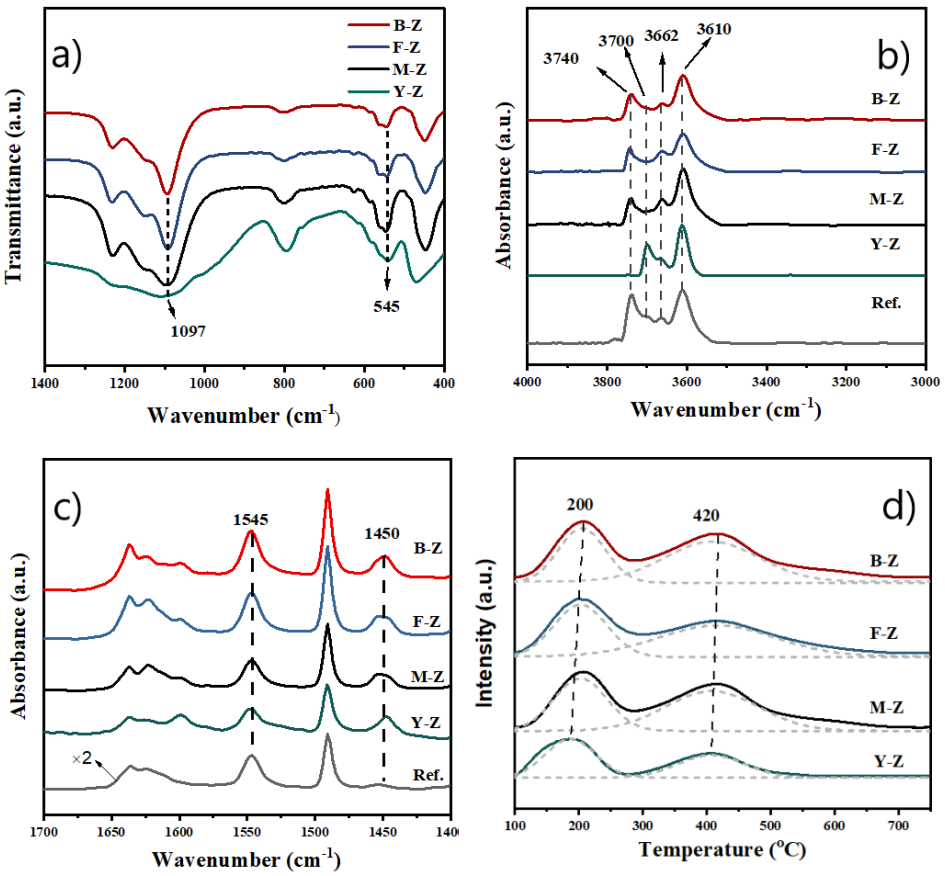

Figure 6. FTIR of the inter-zeolite transformation products: a) in the framework vibrational region; b) the -OH vibrations; c) the adsorbed pyridine; and d) the NH_3-TPD.

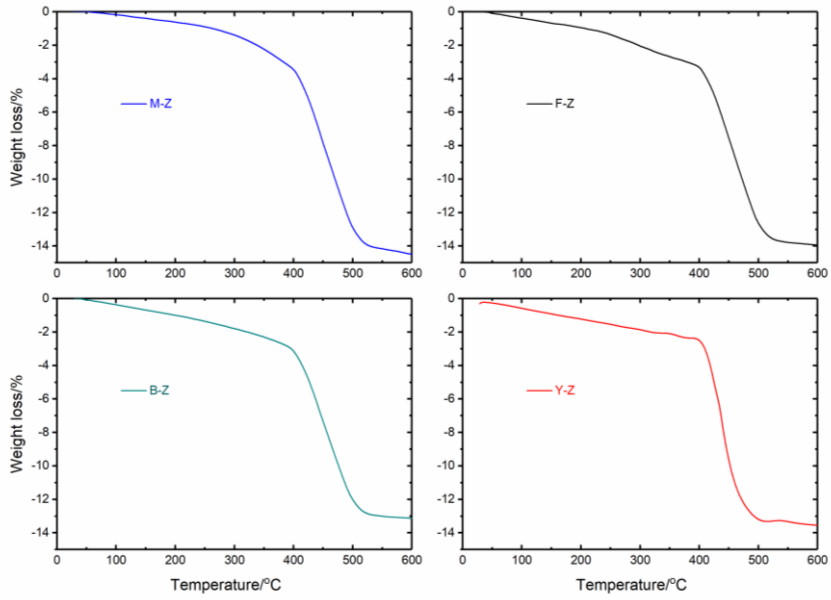

Figure 7. TGA curves of the inter-zeolite transformation products in the acidic medium.

FTIR spectra of dehydrated B-Z, F-Z, and M-Z in the range of hydroxyl group vibrations (Figure 6b) show three sharp absorption bands: the surface silanol -Si-OH at 3740 cm^{-1}, the distorted tetrahedra -Al-OH at 3660 cm^{-1}, and the bridging -Al-(OH)-Si- at 3610 cm^{-1}, i.e., the Brønsted acid sites.[50] The reference ZSM-5 crystallized in the basic medium shows a more intense band at 3740 cm^{-1}, a similar band 3610 cm^{-1}, and a less intense band 3660 cm^{-1}. The spectrum of Y-Z has similar bands at 3610 and 3660 cm^{-1}. But its 3740 cm^{-1} band is extremely weak. Instead, it has a strong peak at 3700 cm^{-1}, which is attributed to the surface terminal -Al-OH and the internal silanols at the connectivity defects. The presence of a big portion of surface Al units, i.e., a serious enrichment of Al atoms at the external surface emphasizes different mechanism of the crystallization of ZSM-5 issued from H-Y in respect to the pentasil-type precursors.

Table 2. Acidic characteristics of the inter-zeolite transformation products and the basic medium synthesized reference sample.

Sample	LAS[a] /mmol/g	BAS[a] /mmol/g	Total[a] /mmol/g	Strong[b] (%)	Weak[b] (%)
B-Z	0.2198	0.7526	0.9724	49.03	50.97
F-Z	0.2232	0.6497	0.8729	48.74	51.26
M-Z	0.1711	0.4444	0.6155	48.54	51.46
Y-Z	0.0790	0.2070	0.2860	44.00	56.00
Ref.	0.0168	0.2721	0.2889	42.99	57.01

[a] FTIR spectra of adsorbed pyridine.
[b] NH_3-TPD.

TG curves of the IZT products in Figure 7 are almost identical. From 425 to 520°C the weight-losses corresponding to the combustion of TPA^+ are between 10-11%. As mentioned above, to balance these cationic charges, an ideal ZSM-5 with the perfect lattice would have a Si/Al ratio of 24 to 27, values touching the limits of the highest Al amount that $|TPA^+|$-ZSM-5 can accommodate. The analyzed values in Table 1 are lower than the theoretical values according to the ideal lattices for the products out of the pentasil-type parents, revealing again the existence of extra-framework Al-species. The ZSM-5 product out of H-Y has a Si/Al ratio higher than the ideal calculation. In this case, framework defects take part in the charge balance, together with F^- ions in the cages and the frameworks.

The acidity of the IZT products has been studied by pyridine adsorption under FTIR (Figure 6c), and by NH_3-TPD (Figure 6d). The results are compared with the reference samples synthesized in the basic medium. The absorption band at 1545 cm^{-1} is related to the pyridinium ion (HPy^+) coordinated to Brønsted acid sites (BAS), while the band at 1450 cm^{-1} corresponds to the pyridine (LPy) coordinatively bonded to Lewis acid sites (LAS). The band at 1490 cm^{-1} is the superposition of the bands of pyridine on Brønsted and Lewis sites.[51, 52] NH_3-TPD shows the strength distributions of these acid sites. Quantitative analysis of the pyridine-adsorbed FTIR spectra and NH_3-TPD results are summarized in Table 2.

There are obvious and fundamental differences between the IZT products, especially the ones out of the pentasil parents, and the reference ZSM-5. First, the total amounts of acid sites

accessible to pyridine are significantly larger in the IZT products out of the pentasils than in the reference ZSM-5. Especially, the former ones have 10 times more LAS than the reference, which implies the existence of significant amounts of extra-framework alumina species in the IZT products. A large amount of LAS in the material is negative from the viewpoint of structure integrity. It comes from the fact that we used precursors with Si/Al ratio lower than that |TPA^+|-ZSM-5 could accommodate in the framework. And the excess Al amounts may be entrapped in the product zeolite cavities. Second, the strength distribution of the acid sites between two types of materials is different, too. When we divide the NH_3-TPD curves into two peaks at 205 and 415°C for the weak and strong sites, respectively, the pentasil IZT products have ca. 50/50 distribution, while the reference ZSM-5 has a ratio of weak and strong acid sites at 57/43. B-Z has more BAS than F-Z and M-Z, while LAS amounts are similar among the three inter-zeolite transformation products. This result might be due to the more favorable configuration of Al-containing species issued from zeolite Beta, where further experimental proof is required to confirm this hypothesis. The acidity of the Y-Z sample assimilates more like the basic medium synthesized reference rather than the pentasil IZT products. It has a similar total acid amount to the reference sample, and a slightly higher portion of LAS, due to defects rather than extra-framework Al-species.

Summarizing FTIR, NH_3-TPD, and NMR results, the IZT ZSM-5 out of the pentasil parents have much more and stronger BAS than the reference material because of their higher crystallinity; and much more LAS, because they have ineligible amounts of extra-framework alumina. These unique features of unusual acidity may find specific catalytic applications in the future. In contrast, The ZSM-5 made from H-Y by longer hydrothermal treatment possesses a similar amount of acid sites as the reference, but the portion of LAS is slightly higher because of the framework torsions and defects.

3.3 The catalytic properties of the IZT products in alcohol dehydration reactions

The impact of different acidity of the IZT ZSM-5 materials was tested in the alcohol dehydration reactions (Figure 8). Methanol dehydration between 100 and 160°C over zeolites yields dimethyl-ether as a single product (Figure 8a). The reaction rate should be proportional to the total amount of acid sites. In Figure 10, this rule is approximately obeyed by the IZT products out of the pentasils: the conversions of MeOH are following the order of B-Z ~ F-Z > M-Z, parallel to the order of the respective acid site concentrations of these materials. However, compared to the reference ZSM-5 synthesized in a traditional basic medium with significantly fewer acid sites, the MeOH conversion also falls in the same range. It is envisaged that other factors, such as crystal sizes and morphology, framework integrity, and related surface hydrophilicity/hydrophobicity, play roles in the experiments. Y-Z has the lowest activity because it has the least amount of acid sites, especially the least amount of strong acid sites.

At 200°C, ethanol dehydration products are ethene and ethyl-ether. Figure 8b illustrates the steady-state conversion of ethanol and the corresponding ethene selectivity. The reference ZSM-5 exhibits 100% conversion and 87% ethene selectivity. B-Z, F-Z, and M-Z have significantly lower activity at their steady states (37%, 82%, and 48%, respectively), with slightly lower ethene selectivity (67%, 82% and 86%). Y-Z has a moderate activity (X=73%) but a significantly lower ethene selectivity (31%). The main product over Y-Z is ethyl-ether. It is plausible to consider that the strong sites of the IZT products become coked at the initial stages of the reaction, and the pores are blocked irregularly.

The dehydration of propanol at 180°C behaves similarly over these materials. The dehydration products include di-n-propyl-ether and propene. Figure 8c shows the propanol conversion and propene selectivity. The reference ZSM-5 has 100% propanol conversion and 68% propene conversion. The pentasil IZT products show around 60% propanol conversion, and the propene selectivity is 61% for B-Z, 50% for F-Z, and 47% for M-Z. Y-Z has a 100% conversion, the ether selectivity of ca. 93%. The stronger acids experience fast deactivation upon contact with the higher alcohol.

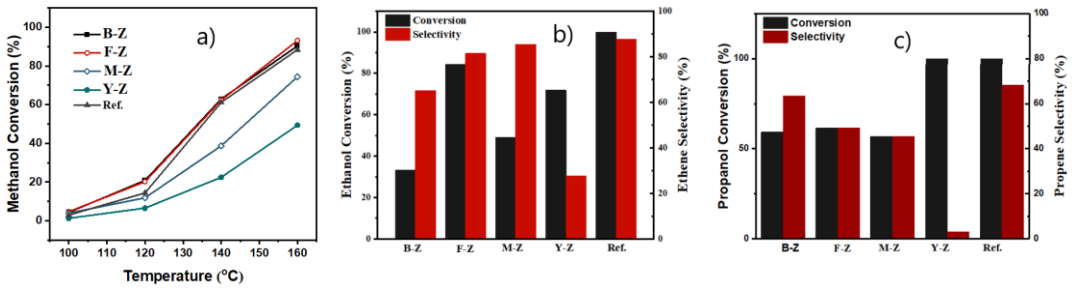

Figure 8. The catalytic performances of the inter-zeolite transformation products, in comparison with the traditional basic reference: a) methanol to dimethyl-ether at 100-160°C; b) ethanol to ethene and ethyl-ether at 200°C; and c) propanol to propene and dipropyl-ether at 180°C.

4. Conclusions

The transformation of zeolite H-Y, H-beta, H-ferrierite, and H-mordenite into ZSM-5 in a strongly acidic fluoride medium was achieved. Highly crystalline products with Si/Al framework ration close to 20 were obtained. Much slower transformation kinetics has been observed for the case of high-silica USY than in the pentasil type precursors. The different crystallization behavior is attributed to the impact of the parent zeolite framework topology. The pentasil-type zeolites, ***BEA**, **FER**, **MOR,** possessing similar structural units to the **MFI**, transform rapidly and generate highly crystalline nano-plates. During the dissolution the common structure units contribute to an inherently fast nucleation. Furthermore, at least a part of the structured linkages containing -Si-O-Al- units are retained during the recrystallization process. In contrast, the **FAU**-type material lacking a common building unit with the target must be dissolved deeper into smaller pieces, which undergo slower nucleation and growth.

The acidic properties of the IZT products from the pentasil parents obtained in an acidic medium display significant differences from the traditional ZSM-5 with similar Si/Al ratios in the concentration, strength, and types of the acid sites. They have much more and stronger BAS than their traditional basic medium synthesized counterparts because of their more ordered crystal lattices. Also, they exhibit much more LAS, because they have ineligible amounts of extra-framework alumina. The ZSM-5 out of USY has a similar amount of acid sites to the traditional ZSM-5, where LAS has a higher portion due to lattice detorsion and defects. These unique features of the unusual acidity may find specific catalytic applications in the future. Tests in alcohol dehydration reactions unveil catalytic behaviors different from a conventional ZSM-5.

CRediT authorship contribution statement

D. Shi: Investigation, Writing – original draft. **G. Fu**: Methodology, Investigation. **A. Omran, K.-G. Haw, L. Zhu, R. Ding, Q. Lang, S. Wang**: Investigation. **Q. Fang, S. Qiu**: Supervision. **X. Yang**: Methodology, Writing – original draft. **V. Valtchev**: Conceptualization, Writing – review & editing, Supervision, Funding acquisition.

Declaration of competing interest

The authors declare that they have no known competing financial interests or personal relationships that could have appeared to influence the work reported in this paper.

Acknowledgments

V.V., S.Q., Q.F. and X.Y. acknowledge the collaboration in the framework of Sino-French International Research Network (IRN) "Zeolites". The ZeoMat Group acknowledges the support by Shandong Energy Institute (SEI S202107), Natural Science Foundation of Shandong Province (ZR2022MB053 and ZR2022QB216). Q.F. thanks the National Natural Science Foundation of China (21571079, 21621001, 21390394, 21571076 and 21571078) for financial supports.

Appendix A. Supplementary Data

Additional materials synthesis details and characterizations are available as:

SupplementaryInformation.pdf

References

1. Y. Li and J. Yu, Emerging applications of zeolites in catalysis, separation and host–guest assembly, *Nature Reviews Materials*, 2021, DOI: https://10.1038/s41578-021-00347-3.
2. Y. Li, L. Li and J. Yu, Applications of Zeolites in Sustainable Chemistry, *Chem*, 2017, **3**, 928-949.
3. M. Zaarour, B. Dong, I. Naydenova, R. Retoux and S. Mintova, Progress in zeolite synthesis promotes advanced applications, *Microporous and Mesoporous Materials*, 2014, **189**, 11-21.
4. C. Martínez and A. Corma, Inorganic molecular sieves: Preparation, modification and industrial application in catalytic processes, *Coordination Chemistry Reviews*, 2011, **255**, 1558-1580.
5. B. Louis and L. Kiwi-Minsker, Synthesis of ZSM-5 zeolite in fluoride media: an innovative approach to tailor both crystal size and acidity, *Microporous and mesoporous materials*, 2004, **74**, 171-178.
6. M. S. Nabavi, M. Zhou, J. Mouzon, M. Grahn and J. Hedlund, Stability of colloidal ZSM-5 catalysts synthesized in fluoride and hydroxide media, *Microporous and Mesoporous Materials*, 2019, **278**, 167-174.
7. S. Singhal, S. Agarwal, S. Arora, N. Singhal and A. Kumar, Solid acids: potential catalysts for alkene–isoalkane alkylation, *Catalysis Science & Technology*, 2017, **7**, 5810-5819.
8. N. Rahimi and R. Karimzadeh, Catalytic cracking of hydrocarbons over modified

ZSM-5 zeolites to produce light olefins: A review, *Applied Catalysis A: General*, 2011, **398**, 1-17.
9. C. Li, A. Vidal-Moya, P. J. Miguel, J. Dedecek, M. Boronat and A. Corma, Selective introduction of acid sites in different confined positions in ZSM-5 and its catalytic implications, *ACS Catalysis*, 2018, **8**, 7688-7697.
10. H. E. Lin and A. N. Ko, Alcohol Dehydrations over ZSM - 5 Type Zeolites, Montmorillonite Clays and Pillared Montmorillonites, *Journal of the Chinese Chemical Society*, 2000, **47**, 509-518.
11. L. Yu, J. Yuan, Q. Zhang, Y. M. Liu, H. Y. He, K. N. Fan and Y. Cao, Propylene from renewable resources: Catalytic conversion of glycerol into propylene, *ChemSusChem*, 2014, **7**, 743-747.
12. G. Busca, Acid catalysts in industrial hydrocarbon chemistry, *Chem. Rev.*, 2007, **107**, 5366-5410.
13. F. Su and Y. Guo, Advancements in solid acid catalysts for biodiesel production, *Green Chemistry*, 2014, **16**, 2934-2957.
14. R. Bulánek, M. Kubů, J. Vaculík and J. Čejka, H/D reactivity and acidity of Brønsted acid sites of MWW zeolites: Comparison with MFI zeolite, *Applied Catalysis A: General*, 2019, **575**, 180-186.
15. J.-L. Guth and P. Caullet, Synthèse des zéolites. Perspectives d'avenir, *Journal de chimie physique*, 1986, **83**, 155-175.
16. J. Guth, L. Delmonte, M. Soulard, B. Brunard, J. Joly and D. Espinat, Synthesis of Al, Si MFI-type zeolites in the presence of F^- anions: Structural and physicochemical characteristics, *Zeolites*, 1992, **12**, 929-935.
17. M. A. Camblor, A. Corma and S. Valencia, Synthesis in fluoride media and characterisation of aluminosilicate zeolite beta, *Journal of Materials Chemistry*, 1998, **8**, 2137-2145.
18. P. Caullet, J.-L. Paillaud, A. Simon-Masseron, M. Soulard and J. Patarin, The fluoride route: a strategy to crystalline porous materials, *Comptes Rendus Chimie*, 2005, **8**, 245-266.
19. M. A. Camblor, L. A. Villaescusa and M. J. Díaz-Cabañas, Synthesis of all-silica and high-silica molecular sieves in fluoride media, *Topics in Catalysis*, 1999, **9**, 59-76.
20. D. Shi, K.-G. Haw, C. Kouvatas, L. Tang, Y. Zhang, Q. Fang, S. Qiu and V. Valtchev, Expanding the Synthesis Field of High-Silica Zeolites, *Angewandte Chemie-International Edition*, 2020, **59**, 19576-19581.
21. X. Yang, E. Dib, Q. Lang, H. Guo, G. Fu, J. Wang, Q. Yi, H. Zhao and V. Valtchev, Silicalite-1 formation in acidic medium: Synthesis conditions and physicochemical properties, *Microporous and Mesoporous Materials*, 2022, **329**, 111537.
22. H. Zhao, Q. Lang, G. Fu, R. Ding, S. Wang, X. Yang and V. Valtchev, Hydrothermal crystallization of clathrasils in acidic medium: Energetic aspects, *Microporous and Mesoporous Materials*, 2022, **333**, 111728.
23. G. Fu, E. Dib, Q. Lang, H. Zhao, S. Wang, R. Ding, X. Yang and V. Valtchev, Acidic medium synthesis of zeolites – an avenue to control the structure-directing power of organic templates, *Dalton Transactions*, 2022, **51**, 11499-11506.
24. K. Gayer, L. Thompson and O. Zajicek, The solubility of aluminum hydroxide in acidic and basic media at 25 C, *Canadian Journal of Chemistry*, 1958, **36**, 1268-1271.

25. J. L. Guth, H. Kessler, J. M. Higel, J. M. Lamblin, J. Patarin, A. Seive, J. M. Chezeau and R. Wey, in *Zeolite Synthesis, ACS Symp. Series 398*, eds. M. L. Occelli and H. E. Robson, ACS, Washington D.C, 1989, pp. 17-38.
26. T. Moteki and R. F. Lobo, A general method for aluminum incorporation into high-silica zeolites prepared in fluoride media, *Chemistry of Materials*, 2016, **28**, 638-649.
27. N. Funase, T. Tanigawa, Y. Yamasaki, N. Tsunoji, M. Sadakane and T. Sano, Thermally stable nanosized LEV zeolites synthesized by hydrothermal conversion of FAU zeolites in the presence of N, N-dimethylpiperidinium cations, *Journal of Materials Chemistry A*, 2017, **5**, 19245-19254.
28. N. A. Khan, D. K. Yoo, B. N. Bhadra, J. W. Jun, T.-W. Kim, C.-U. Kim and S. H. Jhung, Preparation of SSZ-13 zeolites from beta zeolite and their application in the conversion of ethylene to propylene, *Chemical Engineering Journal*, 2019, **377**, 119546.
29. K. H. Møller, M. Debost, L. Lakiss, S. Kegnæs and S. Mintova, Interzeolite conversion of a micronsized FAU to a nanosized CHA zeolite free of organic structure directing agent with a high CO2 capacity, *RSC Advances*, 2020, **10**, 42953-42959.
30. K. Mlekodaj, M. Bernauer, J. E. Olszowka, P. Klein, V. Pashkova and J. Dedecek, Synthesis of the zeolites from SBU: An SSZ-13 study, *Chemistry of Materials*, 2021, **33**, 1781-1788.
31. M. M. Lozinska, E. L. Bruce, J. Mattock, R. G. Chitac, P. A. Cox, A. Turrina and P. A. Wright, Understanding the Anion-Templated, OSDA-Free, Interzeolite Conversion Synthesis of High Silica Zeolite ZK-5, *Chemistry – A European Journal*, 2022, DOI: https://doi.org/10.1002/chem.202201689, e202201689.
32. L. Tang, K.-G. Haw, Y. Zhang, Q. Fang, S. Qiu and V. Valtchev, Fast and efficient synthesis of SSZ-13 by interzeolite conversion of Zeolite Beta and Zeolite L, *Microporous and Mesoporous Materials*, 2019, **280**, 306-314.
33. L. Xu, Y. Yuan, Q. Han, L. Dong, L. Chen, X. Zhang and L. Xu, High yield synthesis of nanoscale high-silica ZSM-5 zeolites via interzeolite transformation with a new strategy, *Catalysis Science & Technology*, 2020, **10**, 7904-7913.
34. J. Zhang, J. Liang, H. Peng, Y. Mi, P. Luo, H. Xu, M. He and P. Wu, Cost-effective fast-synthesis of chabazite zeolites for the reduction of NOx, *Applied Catalysis B: Environmental*, 2021, **292**, 120163.
35. R. Jain, A. J. Mallette and J. D. Rimer, Controlling Nucleation Pathways in Zeolite Crystallization: Seeding Conceptual Methodologies for Advanced Materials Design, *Journal of the American Chemical Society*, 2021, **143**, 21446-21460.
36. S. Goel, S. I. Zones and E. Iglesia, Encapsulation of Metal Clusters within MFI via Interzeolite Transformations and Direct Hydrothermal Syntheses and Catalytic Consequences of Their Confinement, *Journal of the American Chemical Society*, 2014, **136**, 15280-15290.
37. J. Devos, S. Robijns, C. Van Goethem, I. Khalil and M. Dusselier, Interzeolite Conversion and the Role of Aluminum: Toward Generic Principles of Acid Site Genesis and Distributions in ZSM-5 and SSZ-13, *Chemistry of Materials*, 2021, **33**, 2516-2531.
38. P. A. Jacobs and J. A. Martens, in *Studies in Surface Science and Catalysis*, eds. P.

A. Jacobs and J. A. Martens, Elsevier, 1987, vol. 33, pp. 167-215.
39. S. Mintova, N. H. Olson, J. Senker and T. Bein, Mechanism of the transformation of silica precursor solutions into Si-MFI zeolite, *Angewandte Chemie*, 2002, **114**, 2670-2673.
40. W. Dai, C. Kouvatas, W. Tai, G. Wu, N. Guan, L. Li and V. Valtchev, Platelike MFI Crystals with Controlled Crystal Faces Aspect Ratio, *Journal of the American Chemical Society*, 2021, **143**, 1993-2004.
41. C. A. Fyfe, J. H. O'Brien and H. Strobl, Ultra-high resolution 29Si MAS NMR spectra of highly siliceous zeolites, *Nature*, 1987, **326**, 281-283.
42. E. Dib, J. Grand, A. Gedeon, S. Mintova and C. Fernandez, Control the position of framework defects in zeolites by changing the symmetry of organic structure directing agents, *Microporous and Mesoporous Materials*, 2021, **315**, 110899.
43. H. Koller, A. Wölker, L. A. Villaescusa, M. J. Díaz-Cabañas, S. Valencia and M. A. Camblor, Five-Coordinate Silicon in High-Silica Zeolites, *Journal of the American Chemical Society*, 1999, **121**, 3368-3376.
44. Z. S. Lin, D. Chen, H.-Y. Nie, Y. T. A. Wong and Y. Huang, Investigations of the formation of zeolite ZSM-39 (MTN), *Canadian Journal of Chemistry*, 2019, **97**, 840-847.
45. A. Sadoc, M. Biswal, M. Body, C. Legein, F. Boucher, D. Massiot and F. Fayon, NMR parameters in column 13 metal fluoride compounds (AlF3, GaF3, InF3 and TlF) from first principle calculations, *Solid State Nuclear Magnetic Resonance*, 2014, **59-60**, 1-7.
46. G. Scholz and E. Kemnitz, Mechanochemical synthesis of AlF3 with NH4F as fluorinating agent – Does it work?, *Solid State Sciences*, 2009, **11**, 676-682.
47. H. G. Karge and J. Kärger, in *Adsorption and Diffusion*, eds. H. G. Karge and J. Weitkamp, Springer Berlin Heidelberg, Berlin, Heidelberg, 2008, DOI: 10.1007/3829_2008_020, pp. 135-206.
48. G. Coudurier, C. Naccache and J. C. Vedrine, Uses of i.r. spectroscopy in identifying ZSM zeolite structure, *Journal of the Chemical Society, Chemical Communications*, 1982, DOI: 10.1039/C39820001413, 1413-1415.
49. E. M. Flanigen, H. Khatami and H. A. Szymanski, in *Molecular Sieve Zeolites-I*, American Chemical Society 1974, vol. 101, ch. 16, pp. 201-229.
50. A. Palčić and V. Valtchev, Analysis and control of acid sites in zeolites, *Applied Catalysis A: General*, 2020, **606**.
51. M. C. Kung and H. H. Kung, IR studies of NH3, Pyridine, CO, and NO adsorbed on transition metal oxides, *Catalysis Reviews Science and Engineering*, 1985, **27**, 425-460.
52. G. Busca, Acidity and basicity of zeolites: A fundamental approach, *Microporous and Mesoporous Materials*, 2017, **254**, 3-16.